Journal of Experimental Botany, Vol. 52, No. 356,
Compartmentation Special Issue, pp. 631–640, April 2001

Journal of Experimental Botany

Confocal imaging of metabolism *in vivo*: pitfalls and possibilities

M.D. Fricker[1] and A.J. Meyer[2]

Department of Plant Sciences, University of Oxford, South Parks Road, Oxford OX1 3RB, UK

Received 29 July 2000; Accepted 24 November 2000

Abstract

Confocal laser scanning microscopy (CLSM) has had wide application in morphological studies and ion imaging in plants, but little impact so far on biochemical investigations. This position is likely to change as the range of fluorescent probes increases. To illustrate the type of kinetic information that can be obtained using CLSM in an intact, living system, an analysis has been made of the two-step detoxification of monochlorobimane (MCB) following conjugation to glutathione (GSH) by a glutathione *S*-transferase in the cytoplasm and vacuolar sequestration of the fluorescent glutathione *S*-bimane (GSB) by a glutathione *S*-conjugate (GSX) pump. Fluorescence from the cytoplasm and vacuole of individual trichoblasts and atrichoblasts was measured from time-series of (*x, y*) optical sections in the elongation zone of *Arabidopsis* root tips. Intensity changes were calibrated and converted to amounts using compartment volumes, measured by stereological techniques. The data were well described using pseudo-first-order kinetics for the conjugation reaction and either Michaelis-Menten kinetics (Model I), or, as the GSX-pump was operating close to V_{max}, a pseudo-zero-order reaction (Model II), for the GSX-pump. Analysis of 15 individual cells from two roots gave $[GSH]_{cyt}$ in the range 1.8–4 mM. GST activity was relatively constant on a cell basis in one root, but increased markedly in the other, giving a net increase in conjugation activity as cells progressed through the elongation zone. In contrast, GSX-pump activity increased in parallel with the increase in cell size in both roots, effectively maintaining a constant transport activity per unit root length or estimated vacuole surface area.

Key words: Confocal microscopy, glutathione, glutathione *S*-conjugate pump, glutathione *S*-transferase, monochlorobimane.

Introduction

Confocal laser scanning microscopy (CLSM) can be used to collect optical sections, free from out-of-focus blur, from fluorescent probes distributed within fixed or living plant tissues (Gilroy, 1997; Hepler and Gunning, 1998; Roos, 2000; Blancaflor and Gilroy, 2000). The increased contrast achieved in comparison to conventional wide-field fluorescence imaging, greatly improves visualization of cellular and subcellular structures in thin optical sections, furthermore, it is straightforward to obtain 3-D views of the label distribution from a stack of such sections collected with a defined focus increment. Measurements from single optical sections or 3-D volumes can also be repeated in time to visualize and subsequently quantify dynamic events non-invasively in living tissues. Most studies in living plant systems have used CLSM to obtain morphological information, notably in conjunction with specific targeting of green fluorescent protein (GFP) to organelles or cytoskeletal structures (Hepler and Gunning, 1998; Hanson and Köhler, 2001) or, to a lesser extent, to probe physiological parameters such as pH and calcium dynamics (Gilroy, 1997; Roos, 2000). In principle, CLSM should enable *in vivo* measurements of many other parameters

[1] To whom correspondence should be addressed. Fax: +00 44 1865 275074. E-mail: mark.fricker@plants.ox.ac.uk
[2] Present address: Institut für Forstbotanik und Baumphysiologie, Professur für Baumphysiologie, Universität Freiburg, Georges-Köhler-Allee 53, D-79085 Freiburg, Germany.

Abbreviations: CLSM, confocal laser scanning microscopy; FRET, fluorescence resonance energy transfer; GFP, green fluorescent protein; GSB, glutathione *S*-bimane; GSH, glutathione; GST, glutathione *S*-transferase; GSX, glutathione *S*-conjugate; MCB, monochlorobimane; NA, numerical aperture; S/N, signal-to-noise ratio; ROI, region of interest; TIP, tonoplast intrinsic protein; TPLSM, two-photon laser scanning microscopy.

of interest to biochemists and physiologists, including metabolite levels, enzyme kinetics, subcellular compartmentalization or cell–cell partitioning. For example, one goal for this type of technique would be to measure the actual enzyme activities within specific cells, to take into account all the post-translation modification, substrate and cofactor levels, rather than the amount of mRNA and protein determined by Northern and Western blotting, respectively, or RNA and protein (antibody) *in situ* hybridization techniques. The ability to visualize subcellular details compares favourably with other imaging techniques, such as NMR imaging, which can currently achieve in-plane resolution of the order of 50–100 μm at best (Kockenberger, 2001).

Despite the potential benefits from non-invasive confocal imaging, there have been no studies in plants, to the best of our knowledge, that have specifically used CLSM to quantify the activity of a metabolic pathway *in vivo*, and only a handful of papers that have imaged a metabolite, as opposed to an inorganic ion. One major reason for this lack of data is the current paucity of suitable fluorescent probes for organic compounds of interest. This position is expected to change within the next few years with the continuing development of both chemical and protein-based reporters (Haugland, 1999), currently, however, this field is at a very embryonic stage. Thus in this paper, a number of points are considered that the authors believe will be pertinent to confocal imaging of metabolism in the future and there is an illustration of the type of information that can be obtained from a combination of *in vivo* CLSM and modelling techniques, using GSH-dependent detoxification of a model substrate, monochlorobimane (MCB), as an example.

What types of probe are available to image metabolism?

The simplest imaging approach in plant cells would be to capitalize on the numerous intrinsic auto-fluorescent compounds, such as NAD(P)H, chlorophylls, anthocyanins, flavoproteins, phenolics, and lignins, particularly if UV-excitation is available (Hutzler *et al*., 1998). For example, in animal tissues the redox state of the NADH pool has been measured from auto-fluorescence of the reduced nucleotides using UV-CLSM or two-photon laser scanning microscopy (TPLSM) (Piston *et al*., 1995) and used to infer changes in glucose metabolism (Bennett *et al*., 1996). In plants, there is one report measuring changes in redox state *in vivo* from changes in reduced nucleotide fluorescence under hypoxia (Roberts *et al*., 1984). These authors used photometry rather than imaging, but in the future, redox imaging may provide a powerful adjunct to many biochemical analyses if the weak signals from reduced pyridine nucleotides can be effectively separated from the range of other UV-excitable compounds present and quantified accurately.

In the case of fluorescent products of secondary metabolism such as the anthocyanins, flavonoids, phenolics, and lignins, their tissue and cellular localization can be readily observed *in vivo*, however changes in their concentration occur over such relatively long time periods suggesting that kinetic analysis may only have limited use. In contrast, the most successful application of fluorescent techniques to understanding metabolism is based on analysis of rapid (ms) transients in chlorophyll fluorescence and the inferences that can be drawn on the electron flow from the reaction centres and ultimately the activity of the dark reactions (Baker *et al.*, 2001). The amount of chlorophyll fluorescence inversely tracks both the flow of electrons from the reaction centres and the amount of non-photochemical quenching, and has been used as a powerful tool to monitor parameters, such as the photochemical yield of PSII, over a range of different spatial resolutions. Thus, imaging systems have been developed that operate at the tissue level (Genty and Meyer, 1994) down to single chloroplasts within cells in intact leaves (Oxborough and Baker, 1997). CLSM would give an additional level of spatial resolution to these studies, however, the temporal resolution required for quantitative analysis of fluorescence transients in the ms range and the reduced signal-to-noise ratio (S/N) possible with rapid scanning have so far discouraged development of quantitative confocal analysis. Nevertheless, qualitative imaging of chlorophyll autofluorescence does provide a ready marker of chloroplast morphology or disposition (Tlalka *et al*., 1999).

For non-fluorescent compounds, two routes are available to develop a fluorescent assay appropriate for confocal imaging and analysis. The first approach involves a probe that is itself a substrate for one of the enzymes in the pathway and exhibits a change in its fluorescent properties during the reaction. A considerable range of fluorescent substrates or compounds that release a fluorescent product is available (Haugland, 1999). So far in plants, most if not all of these compounds have been used to report the presence of a particular enzyme activity in a given compartment (Swanson *et al*., 1998), or used as a measure of cell viability, rather than as a route to analyse the kinetics of specific enzymes or fluxes through the pathway.

The second approach involves a probe that interacts specifically, but reversibly, with the target but does not participate in the reaction. This class of probes is typified by the ion reporters that reversibly bind to an ion of interest with a particular dissociation constant (k_d) and selectivity (Roos, 2000). This type of probe can provide information on the steady-state concentration of the target, but not directly its rate of synthesis or consumption. Based on the precedents from the ion-imaging field,

the most useful reversible probes, termed ratio probes, exhibit a shift in their excitation or emission spectrum between the free and bound forms. The shift in spectrum can be readily measured as a ratio between images or average intensities measured at two wavelengths, typically corresponding to the peak wavelengths for the free and bound forms (Grynkiewicz *et al*., 1985). The ratio provides a convenient means to correct for changes in dye concentration, pathlength, photobleaching or leakage (Bright *et al*., 1989). Single wavelength probes only show changes in intensity on binding with no spectral shift. In these cases, it is more difficult to separate changes in fluorescence arising from changes in target concentration versus changes in the dye concentration as both translate into a change in intensity. The number of probes for ions is increasing rapidly as it is possible to design specific binding sites to co-ordinate the metal ligands. Probes for anions have been slower to develop and there are still many anions that cannot be measured with these techniques. There are even fewer probes for organic molecules currently available. Sophisticated probes have been developed for some metabolites, such as cAMP (Adams *et al*., 1991, 1999). In this case, specificity for cAMP is achieved by using the cAMP binding site of the regulatory subunit of protein kinase A. Binding of cAMP triggers dissociation of the fluorescently-tagged subunits of the protein kinase A complex that can be measured as a decrease in fluorescence resonance energy transfer (FRET) between the labelled subunits. Changes in FRET between spectral variants of GFP has also been exploited to design transgenic ratio indicators for calcium (Miyawaki *et al*., 1997, 1999). The use of FRET promises to be an area of great potential in the development of metabolite probes by, for example, incorporating other ligand-binding sites or substrate sites (Heim and Tsien, 1996) that alter the extent of coupling between spectral variants of GFP.

What spatial and temporal resolution can be achieved?

Assuming a suitable probe is available, it is pertinent to ask what level of spatial and temporal resolution can actually be achieved in practice using CLSM in comparison to other techniques. In theory, the smallest volume that can be conveniently imaged in a confocal microscope is around $0.2 \times 0.2 \times 0.6$ μm in x, y and z, respectively, for an oil-immersion PlanApo lens with a numerical aperture of 1.4 (Pawley, 1995). In physiological experiments, a number of compromises are usually required to reduce phototoxicity and keep the specimen alive and functioning as close to normal as possible. This might for example include the use of a lower numerical aperture (NA) long-working distance water-immersion lens to allow deeper penetration into the tissue and reduce the mis-match in refractive index between specimen, immersion medium and coverslip, and/or reducing the level of confocality to increase the signal-to-noise (S/N) ratio primarily at the expense of optical section thickness. Averaging over several pixels or successive frames can be used to increase the S/N ratio further, but clearly at the expense of spatial and temporal resolution. For quantitative analysis, average intensities from even larger regions-of-interest (ROIs) are usually used to increase the S/N ratio further, although the initial spatial resolution is essential to ensure the correct compartments are selected. Increasing the excitation intensity to get more signal results in more photobleaching, photodamage and phototoxicity. This is not usually an option if the specimen is to remain healthy.

With these caveats in mind, a typical figure for the spatial resolution achieved during ion imaging, for example, might be around $1.2 \times 1.2 \times 1.2$ μm in (x, y and z) after a 3×3 averaging filter applied to single optical sections. This resolution is adequate to separate larger organelles such as the nucleus, vacuole and chloroplasts, but makes spatial separation of signals from cytoplasm, apoplast, mitochondria, Golgi, and ER very much more difficult if there is label or autofluorescence present in more than one compartment.

The temporal resolution that can be achieved is also variable. The scan speeds of current confocal instruments are very impressive, typically with pixel sampling in the μs range, line scans in the ms range and full framing rates in the seconds range. Specialist instruments can run at higher speeds, with framing rates between 10 and 25 Hz. In practice, there has to be a trade-off between speed, spatial resolution and S/N. In this respect plants are particularly awkward, as the exceedingly high rate of cytoplasmic streaming can limit the amount of frame averaging that is possible without getting movement artefacts. The development of scan systems that allow single-frame sampling at slower scan speeds, line averaging and/or variable frame sizes are likely to have a beneficial impact in this area. Some measurements of rapid Ca^{2+} dynamics in plants have used sampling in the ms range (Goddard *et al*., 2000), however, most time sequences are typically sampled at 1–30 s intervals. The total exposure time is limited and represents a compromise between sampling frequency and experiment duration due to problems with phototoxicity.

Although confocal imaging has the potential to pick-up fluorescence from deep within tissues, refractive index changes, light scattering and absorption all serve to degrade the focus of the excitation beam and spread the fluorescence that is emitted. Unfortunately, the resulting blurred signal is still efficiently rejected by the confocal aperture giving a quite pronounced decrease in intensity with depth into the sample. Around 50 μm appears to

be a practical limit for intact, living plant specimens for CLSM. Techniques such as multi-photon microscopy (Denk *et al*., 1990; Piston, 1999) also provide optical sectioning, but do not require a pinhole and should give better depth penetration. To provide a quantitative estimate of the fluorescence requires a means to account for the loss of signal with depth into the specimen. One route is to use a theoretically determined function (Török *et al*., 1997), but it is difficult to envisage a practical way to apply this approach to biological specimens. A second approach involves determination of some form of empirical attenuation correction that partially restores the signal intensity (White *et al*., 1996; Fricker *et al*., 1997, 2000; Gray *et al*., 1999).

Analysis of the glutathione-dependent xenobiotic detoxification pathway *in situ*

The following section illustrates the type of metabolic physiology that can be undertaken using CLSM to follow the detoxification of a model xenobiotic, monochlorobimane (MCB), following conjugation of the xenobiotic to glutathione (GSH) in the cytoplasm by a glutathione *S*-transferase (GST) (Fig. 1). The glutathione then acts as a molecular tag to target the conjugate to the vacuole via a glutathione *S*-conjugate (GSX) pump (Coleman *et al*., 1997*a*, *b*; May *et al*., 1998; Rea *et al*., 1998; Swanson *et al*., 1998). The requirement for a GST to achieve appreciable rates of conjugation *in vivo* confers specificity for MCB-labelling of GSH compared to other low molecular weight thiols or protein thiols (Coleman *et al*., 1997*b*; AJ Meyer and MD Fricker, unpublished results). MCB is not fluorescent until conjugation to GSH displaces the chloride leaving group and gives rise to a fluorescent glutathione *S*-bimane (GSB). Although the peak excitation of GSB is around 395 nm, with a broad emission around 477 nm, GSB can be imaged with excitation at 442 nm using CLSM (Fricker *et al*., 2000) or at 770 nm using TPLSM (Meyer and Fricker, 2000). The combination of specific labelling and high-resolution imaging enables analysis of the detoxification capacity of each individual cell in a tissue and mapping how this alters during development.

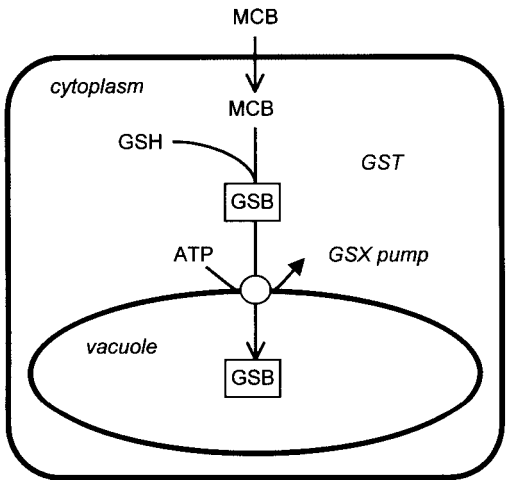

Fig. 1. Schematic diagram of the glutathione-based detoxification pathway in plants. Monochlorobimane (MCB) is used as a model substrate for conjugation to glutathione (GSH) by a glutathione *S*-transferase (GST) in the cytoplasm and subsequent sequestration in the vacuole by a glutathione *S*-conjugate (GSX) pump.

This technique has been used to examine the pattern of GSH-dependent detoxification activity in epidermal cells at the root tip of intact *Arabidopsis* seedlings. Epidermal cells in *Arabidopsis* roots are cut off into files by divisions of initial cells adjacent to the quiescent centre and progress through well-defined stages of elongation and differentiation into trichoblasts and atrichoblasts with increasing distance from the root tip (Dolan *et al*., 1993, 1994). During this developmental sequence, the lytic vacuole is formed, possibly by fusion of very small provacuoles initially into a network of strands and eventually into a single large central vacuole (Jauh *et al*., 1999). In addition, other types of vacuole may be present in some root cells distinguished by their different complement of tonoplast intrinsic protein (TIP) isoforms, lectins and proteases (Paris *et al*., 1996; Jauh *et al*., 1999). Given the proposed importance of vacuolar sequestration of glutathionated xenobiotics in the GSH-detoxification pathway (Coleman *et al*., 1997*a*; Rea *et al*., 1998), it was of interest to determine how the activities of GSTs and GSX-pumps map onto the development of the vacuolar system. To address this question, the rate of GSB formation in the cytoplasm and the rate of sequestration into the vacuole for individual cells in the epidermis at varying stages of development have been measured. Experimental details of the labelling and imaging conditions are given elsewhere (Fricker *et al*., 2000).

The level of fluorescence initially increases in the cytoplasm of all cells in the root observed in single optical sections followed over time (Fig. 2). Some of the label is transported into the vacuole, giving an increase in vacuolar fluorescence and eventually leading to a reduction in cytoplasmic fluorescence. In general, the smallest cells with the highest cytoplasm-to-vacuole ratios showed the greatest increase in vacuolar fluorescence.

To analyse the data, it has been assumed that the conjugation and sequestration reactions can be described as a two-step pathway (1).

$$[\mathrm{GSH}]_{\mathrm{cyt}} + [\mathrm{MCB}]_{\mathrm{cyt}} \xrightarrow{\mathrm{GST}} [\mathrm{GSB}]_{\mathrm{cyt}} \xrightarrow{\mathrm{GSX}} [\mathrm{GSB}]_{\mathrm{vac}} \quad (1)$$

These estimates of $[\mathrm{GSB}]_{\mathrm{cyt}}$ and $[\mathrm{GSB}]_{\mathrm{vac}}$ are based on the average fluorescence (F) measured from manually-defined ROIs in each compartment for each complete cell in the field of view (Fig. 3). To express fluorescence levels in

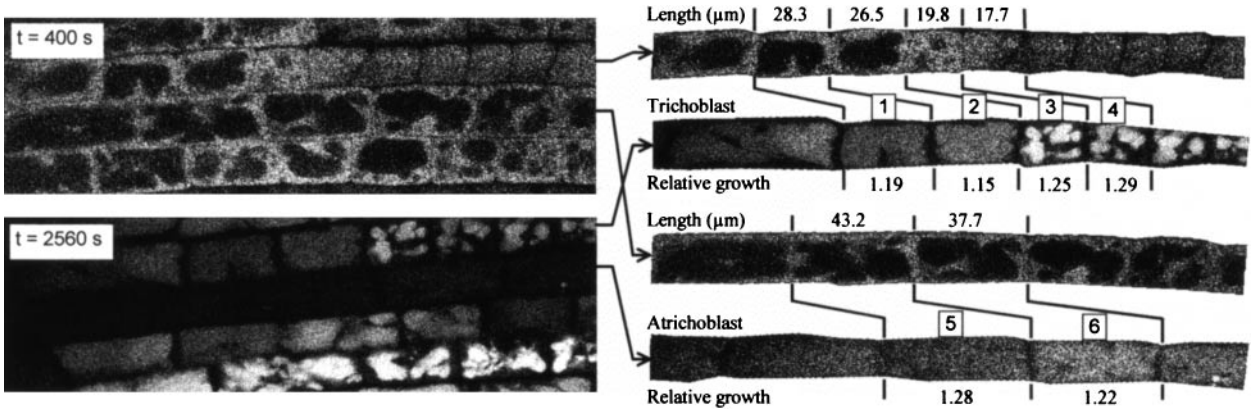

Fig. 2. Confocal imaging of glutathione conjugation to monochlorobimane in intact roots. Glutathione in roots of intact, 5–7-d-old seedlings of *Arabidopsis* was labelled with 100 μM monochlorobimane (MCB) to give a fluorescent glutathione *S*-bimane (GSB) conjugate and imaged as a time-series of optical sections collected at 20 s intervals over about 45 min with excitation at 442 nm. Two representative images are shown after 400 s of labelling, when the fluorescence from the GSB was predominantly cytoplasmic, and 2560 s of labelling, when much of the signal was transferred to the vacuole. The shifts in cell position and cell size arise from the continued growth of the root during the experiment. To make it easier to track changes in individual cells, adjacent trichoblast and atrichoblast cell files have been extracted, normalized for intensity and labelled with their initial length (μm) and their relative growth rate as a fraction of their starting length. In total 12 trichoblast and 4 atrichoblast cells from two different roots were analysed. Scale bar=50 μm.

terms of GSB concentration requires subtraction of the average background signal (F_{back}) and calibration against the average fluorescence of GSB standards (F_{std}) imaged under the same conditions according to equations (2) and (3).

$$[GSB]_{cyt} = \frac{(\overline{F}_{cyt} - \overline{F}_{back})}{(\overline{F}_{std} - \overline{F}_{back})} \quad (2)$$

$$[GSB]_{vac} = \frac{(\overline{F}_{vac} - \overline{F}_{back})}{(\overline{F}_{std} - \overline{F}_{back})} \quad (3)$$

The authors believe that the calibration is appropriate to both compartments, despite their differing microenvironments, as the fluorescence from GSB is not markedly affected by changes in pH, ionic strength or viscosity (Meyer and Fricker, 2000). Ideally, an additional correction should be included to compensate for the amount of signal attenuation with depth into the tissue (White *et al.*, 1996). To date, an empirical correction for *Arabidopsis* roots imaged with a 25×0.85 NA PlanApo multi-immersion lens has been experimentally determined (Fricker *et al.*, 2000), but only roughly estimated an 8% loss in signal for the epidermal cells using the 60×1.4 NA PlanApo oil-immersion lens in roots (Meyer and Fricker, 2000). Comparable attenuation levels in epidermal tissues of *Commelina* (White *et al.*, 1996) give a 10–15% loss of signal in at the depth equivalent to the mid-plane of the cells. Thus the true values of the GSB concentrations may be up to 8–15% higher than those presented here. Although this will affect the absolute concentrations and rates in the following analysis, the trends observed between different cells will still be maintained.

The change in cytoplasmic GSB concentration over time ($d[GSB]_{cyt}/dt$), in units of mol l^{-1} $time^{-1}$, will reflect the balance between the rate of conjugation and the rate of sequestration into the vacuole. In addition, as the cells under examination are still alive and elongating, cell expansion during the assay adds a volume-dependent decrease in the apparent concentration (4).

$$\frac{d[GSB]_{cyt}}{dt} = \frac{rate\ of\ conjugate\ formation - vacuolar\ transport\ rate}{relative\ increase\ in\ cell\ size\ with\ growth} \quad (4)$$

If it is assumed that the concentration of MCB remains constant during the experiment, then the conjugation reaction becomes pseudo-first order for GSH. For simplicity, it has been assumed that both the GST and GSX-pump exhibit Michaelis-Menten kinetics, thus equation 2 can be expressed as (5):

$$\frac{d[GSB]_{cyt}}{dt} = \left(\frac{V_{max}^{app,GST}[GSH]_{cyt}}{K_M^{app,GST} + [GSH]_{cyt}} - \frac{V_{max}^{app,GSX}[GSB]_{cyt}}{K_M^{app,GSX} + [GSB]_{cyt}} \right) \times \frac{1}{relative\ growth} \quad (5)$$

In practice, it was found that the GST appears to operate around or below $K_M^{app,GST}$ so the first term approximates to a first-order rate equation, with k_1^{GST} representing the first-order rate constant (6):

$$\frac{d[GSB]_{cyt}}{dt} \approx \left(k_1^{GST}([GSH]_{cyt}) - \frac{V_{max}^{app,GSX}[GSB]_{cyt}}{K_M^{app,GSX} + [GSB]_{cyt}} \right) \times \frac{1}{relative\ growth} \quad (6)$$

The concentration of GSH in the cytoplasm over time is not known, however it is stoichiometrically related to

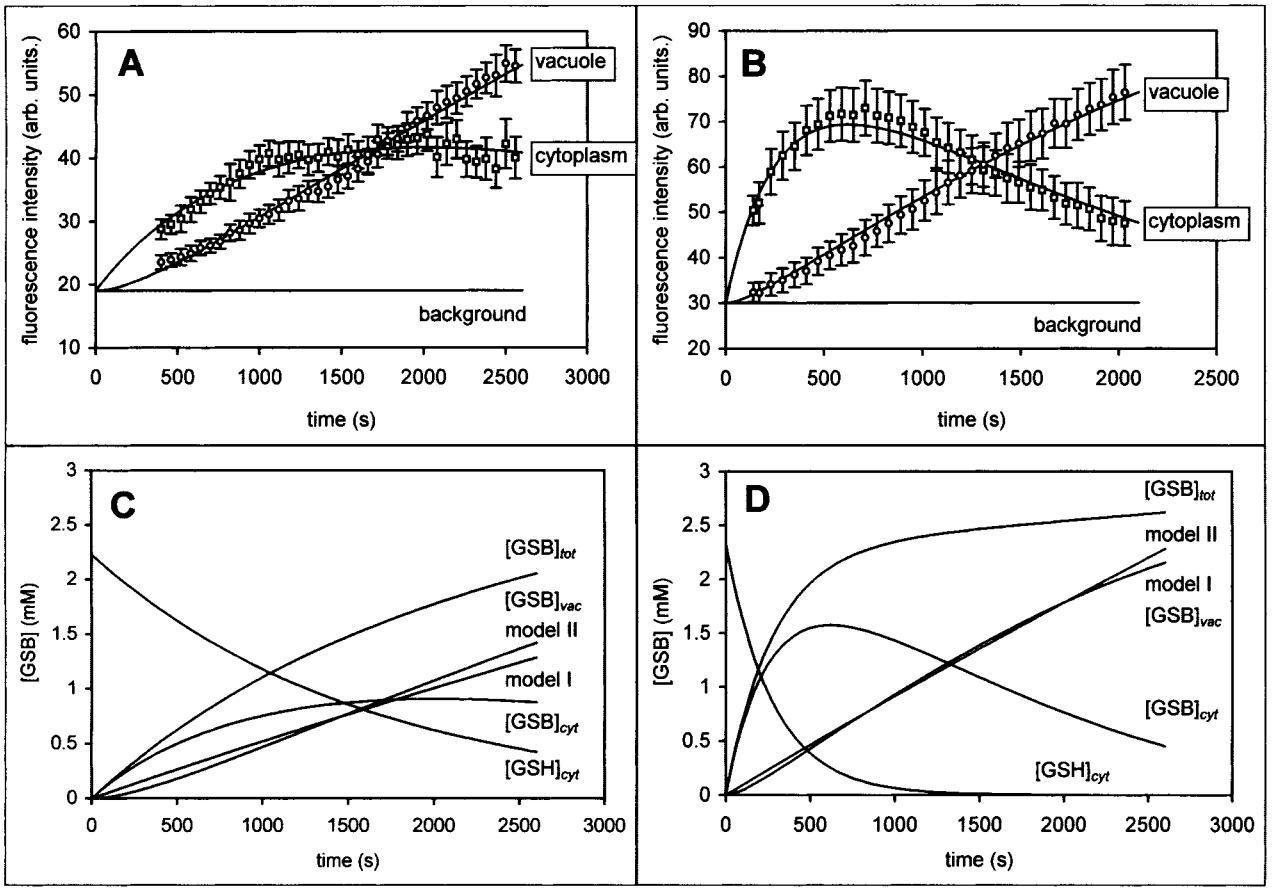

Fig. 3. Time-course measurements of cytoplasmic and vacuolar GSB fluorescence. Changes in the average cytoplasmic fluorescence (□) and vacuolar fluorescence (○) are shown for trichoblast 2 in Fig. 2 (A) and a slightly larger trichoblast (38.5 μm long) from the second root (B). Each value represents a mean and its associated standard deviation. The solid lines fitted to the data represent the simulated time-course following optimization against a two step model with the activity of the GST, modelled as a pseudo-first-order reaction, and the activity of the GSX-pump, modelled using Michaelis-Menten kinetics (Model I). The horizontal line represents the average background intensity. The relatively minor differences between Model I and Model II, in which the GSX-pump is represented as a pseudo-zero-order reaction, for the vacuolar GSB concentration is shown in (C) and (D), along with the predicted changes in cytoplasmic GSH concentration and total GSB formation.

the initial GSH concentration ($[GSH]_0$) present in the cytoplasm and the amount of GSB formed, thus equation (6) can be expressed as (7):

$$\frac{d[\mathrm{GSB}]_{\mathrm{cyt}}}{dt} \approx \left(k_1^{\mathrm{GST}}([\mathrm{GSH}]_0 - [\mathrm{GSB}]_{\mathrm{cyt}}) - \frac{V_{\mathrm{max}}^{\mathrm{app,GSX}}[\mathrm{GSB}]_{\mathrm{cyt}}}{K_{\mathrm{M}}^{\mathrm{app,GSX}} + [\mathrm{GSB}]_{\mathrm{cyt}}} \right) \times \frac{1}{\textit{relative growth}} \tag{7}$$

This combination of a first-order conjugation reaction and Michaelis-Menten kinetics for sequestration is referred to as Model I. It has also been found under the assay conditions used here that the GSX pump is rapidly driven close to its maximum rate, so a second model (Model II) was set up in which the second term in the equation is represented by a zero-order reaction equal to $V_{\mathrm{max}}^{\mathrm{app,GSX}}$ (8).

$$\frac{d[\mathrm{GSB}]_{\mathrm{cyt}}}{dt} \approx (k_1^{GST}([\mathrm{GSH}]_0 - [\mathrm{GSB}]_{\mathrm{cyt}}) - V_{\mathrm{max}}^{\mathrm{app,GSX}}) \times \frac{1}{\textit{relative growth}} \tag{8}$$

The change in vacuolar GSB concentration over time ($d[\mathrm{GSB}]_{\mathrm{vac}}/dt$) will reflect the vacuolar transport rate and the dilution (or concentration) arising from the difference in the relative volumes of cytoplasm and vacuole. The vacuolar concentration will also be affected by any increase in overall cell volume due to cell growth (9):

$$\frac{d[\mathrm{GSB}]_{\mathrm{vac}}}{dt} = \frac{\textit{vacuolar transport rate} \times \textit{cytoplasm to vacuole volume ratio}}{\textit{relative increase in cell size with growth}} \tag{9}$$

The volumes of the cytoplasm (V_{cyt}) and vacuole (V_{vac}) were measured using stereological techniques (Howard

and Reed, 1998; Meyer and Fricker, 2000) in parallel experiments. The changes in both values with increasing cell length are shown for trichoblasts (Fig. 4A) and atrichoblasts (Fig. 4B). Quadratic regression equations were fitted to these data and used to calculate the interpolated values of V_{cyt} and V_{vac} for each of the cells in this study. Including the cytoplasm-to-vacuole volume ratio gives equation (10) for the Michaelis-Menten model of the GSX pump and equation (11) for the simplified zero-order model:

$$\frac{d[\mathrm{GSB}]_{vac}}{dt} = \frac{V_{max}^{app,GSX}[\mathrm{GSB}]_{cyt}}{K_M^{app,GSX} + [\mathrm{GSB}]_{cyt}} \times \frac{V_{cyt}}{V_{vac}} \times \frac{1}{relative\ growth} \quad (10)$$

$$\frac{d[\mathrm{GSB}]_{vac}}{dt} = V_{max}^{app,GSX} \times \frac{V_{cyt}}{V_{vac}} \times \frac{1}{relative\ growth} \quad (11)$$

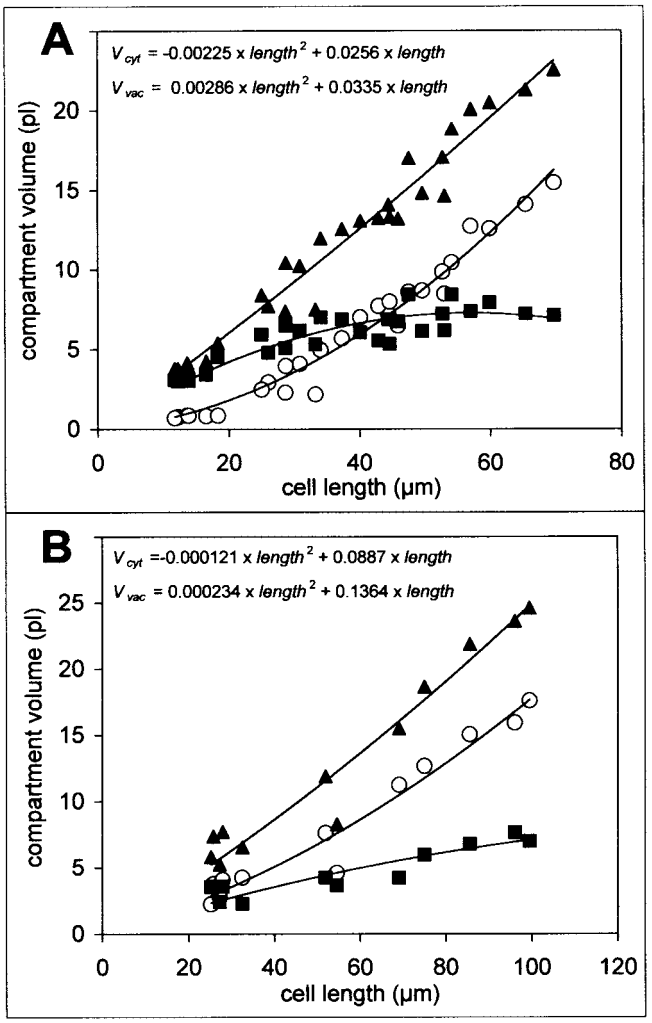

Fig. 4. The relationship between cytoplasmic and vacuolar volume for trichoblast and atrichoblasts in the elongation zone. Serial optical sections were collected with a *z*-focus increment of 1 µm through roots labelled with MCB using 2-photon laser scanning microscopy with excitation at 770 nm. A uniformly spaced set of sections were extracted from a randomised start plane and the volume of the cytoplasm (■) and vacuole (○) were measured for individual trichoblast (A) and atrichoblast (B) cells in the elongation zone using the Cavalieri estimator (Stereology 4.5, Kinetic Imaging, Liverpool, UK). The total volume (▲) was calculated as the sum of the cytoplasm and vacuolar components. The data were fitted with quadratic functions and the resulting equations shown for each panel were used to as an empirical model of the relationship between compartment volume and cell length. Each marker represents data from a single cell. Cells were taken from seven different roots.

Whilst concentration terms are appropriate to represent the apparent affinities of, for example, the GSX-pump in Model I, the overall activity of the two enzymes is better expressed in units of amount rather than concentration. In both Model I and Model II, the activity of the GST is described by a single rate constant, thus in order to allow comparison between different cells, the initial GST activity has been calculated at the prevailing $[\mathrm{GSH}]_{cyt}$ for each cell, using V_{cyt} to convert concentrations into amounts (12).

$$GST\ activity\ (\mathrm{fmol\ cell^{-1}\ min^{-1}}) = k_1^{GST}[\mathrm{GSH}]_0 V_{cyt} \quad (12)$$

As the GSX-pump is operating close to V_{max}, the method simply was to multiply by V_{cyt} to convert this parameter to units of fmol cell^{-1} min^{-1} (13).

$$GSX\ activity\ (\mathrm{fmol\ cell^{-1}\ min^{-1}}) = V_{max}^{app,GSX} V_{cyt} \quad (13)$$

For each of the cells shown in Fig. 2, the differential equations (7) and (10) for Model I or (8) and (11) for Model II, were solved numerically using the 4th order Runge-Kutta method (ModelMaker, Cherwell Scientific Publishing Ltd, Oxford) and optimized iteratively against the cytoplasmic and vacuolar GSB concentrations determined from equations (2) and (3) with k_1^{GST}, $[\mathrm{GSH}]_0$, $V_{max}^{app,GSX}$, and $K_M^{app,GSX}$ as variables used in the optimization. The output from Model I and Model II are presented for two cells in Fig. 3.

The activities of the GST and GSX-pump in fmol min^{-1} cell^{-1} were calculated from the optimized model according to equations (12) and (13), respectively, and data for 12 trichoblast and 4 atrichoblast cells from overlapping regions in the elongation zone of two different roots are summarised in Fig. 5. Cytoplasmic $[\mathrm{GSH}]_{cyt}$ levels varied between 1.8–4 mM (Fig. 5A), similar to previous reports (Fricker *et al.*, 2000; Meyer and Fricker, 2000). There was little difference between the means for trichoblasts of the two roots (2.55 ± 0.55 mM compared to 2.60 ± 0.65 mM). The pooled mean for the atrichoblasts was higher (3.51 ± 0.65 mM), but the sample size is currently very low as fewer entire atrichoblasts were present in each field of view. The initial GST activity, based on the product of k_1^{GST}, $[\mathrm{GSH}]_{cyt}$ and V_{cyt}, increased on a cell basis with increasing cell size (Fig. 5B).

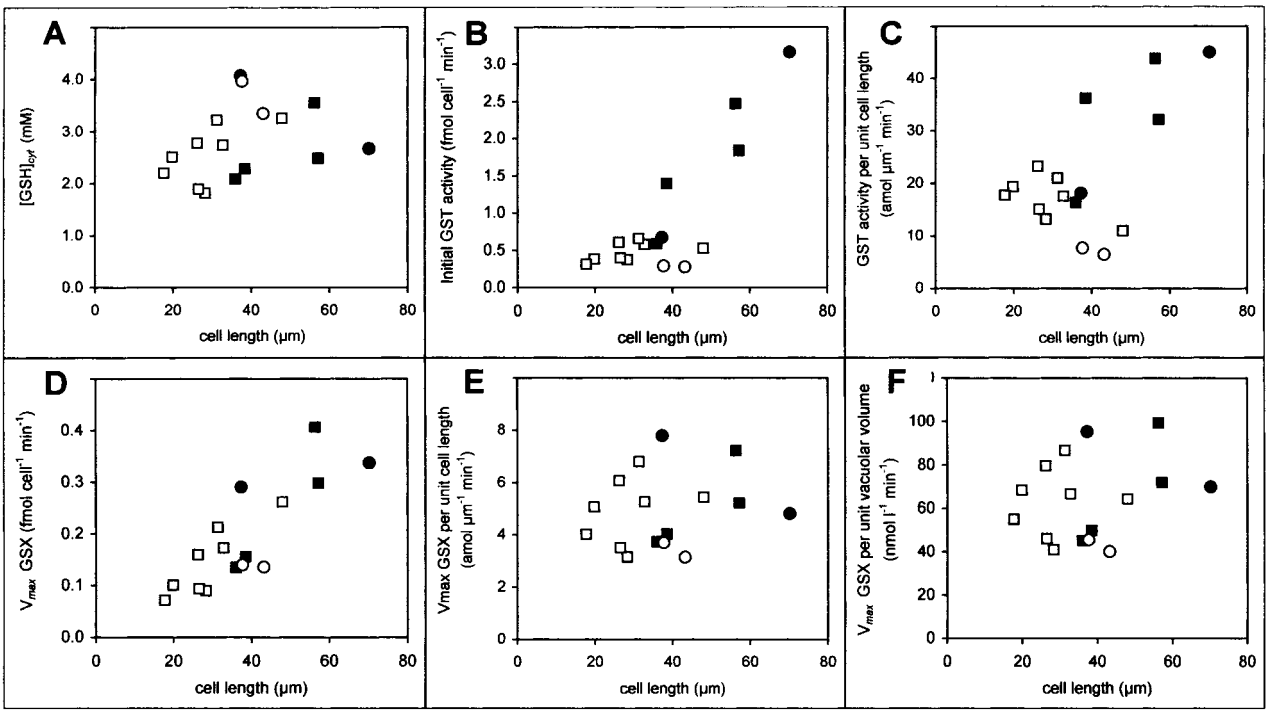

Fig. 5. Prediction of the activity of the glutathione detoxification pathway *in vivo* from simulation modelling of the changes in GSB fluorescence. The cytoplasmic glutathione concentration $[GSH]_{cyt}$ was estimated by optimization of Model II against the average cytoplasmic and vacuolar GSB concentrations measured from trichoblast (□, ■) and atrichoblast (○, ●) cells of two different roots, represented by open and closed symbols (A). Concentrations ranged from about 1.8 mM to 4 mM, but there was little evidence for a change in $[GSH]_{cyt}$ with cell length. The initial GST activity was calculated for each cell based on the pseudo-first-order rate constant for the conjugation reaction, the initial $[GSH]_{cyt}$ and the cytoplasmic volume (B). There appears to be a difference in the behaviour of the two roots, with relatively little change in GST activity with increasing cell length for the first root (open symbols), compared to a substantial increase in GST activity for the second root (closed symbols). This difference becomes even more pronounced when the data are plotted as GST activity per micron cell length (C). The activity of the GSX-pump also increases with increasing cell length, but this time in a similar manner for both roots (D). When expressed as activity per unit cell length (E) or against the two-thirds power of the vacuolar volume as an estimate of tonoplast surface area (F), the GSX activity remains relatively constant with increasing cell size.

To assess the significance of this observation for the ability of the plant to detoxify xenobiotics, the GST activity was expressed per unit length of root (Fig. 5C). There appears to be a difference in the behaviour of the two roots on this basis. In one (Fig. 5C, open symbols), the GST activity falls per unit length, in the other root (Fig. 5C, closed symbols), there is a marked increase in GST activity per unit length. This is reflected in the two cells shown in Fig. 3, which were chosen to represent a cell with a relatively low rate of conjugation versus sequestration (Fig. 3A, C) compared to a cell with a high rate of conjugation from the second root (Fig. 3B, D). Unfortunately, the spread of cell lengths in the two roots only overlaps over a limited range making it difficult to be certain these trends would be maintained over identical developmental regions of the root. In addition, with analysis of only two roots it would be premature to draw any conclusions from this difference except to point out the variability uncovered by quantitative analysis of individual specimens that would be lost in an average measurement based on conventional biochemical extraction and assay techniques.

The apparent V_{max} of the GSX-pump also increases on a cell basis with increasing cell length (Fig. 5D), however, in this case, the activity appears to match the rate of cell elongation, when expressed per unit length of root (Fig. 5E), or against the two-thirds power of the vacuolar volume as an approximation to the tonoplast surface area (Fig. 5F).

Summary and projections

The single most important contribution that this type of analysis can make to our understanding of metabolism is a representation of enzyme activities in identifiable cell types where the environmental context such as pH, ionic strength, substrate, and co-factor concentrations closely approximate to the conditions prevailing *in vivo*. There are, however, a number of significant points to be considered before this can be recommended as a useful, routine approach.

(1) First, the number of probes that are currently available for *in vivo* histochemistry is very low. The

majority are fluorescent substrates or products for cleavage reactions catalysed by esterases, lipases or proteases, rather than probes useful to track primary metabolic pathways.

(2) Second, the analysis is very time-consuming, requiring manual (and subjective) measurement of a number of different parameters, such as average intensities from selected ROIs, attenuation corrections and compartment volumes, each with its associated error. There are, as yet, very few generic or semi-automated protocols for these analyses that can be reliably transferred between different biological systems or even between different microscope configurations.

(3) Third, although some parameters can be considered in isolation, the most relevant ones are derived as outputs from the simulation model and therefore subject to the normal caveats associated with such modelling approaches.

(4) Fourth, by measuring rates in an intact system, it is very much more difficult to bring many of the relevant parameters under experimental control or to provide, for example, the necessary range of substrate concentrations to give robust estimates of the kinetic parameters of the enzymes.

Thus to develop this analysis further, it might be possible to manipulate the original level of GSH in the cytoplasm to generate a progress curve over a greater substrate range for the GST and, thus define an apparent K_m and V_{max} rather than just the pseudo-first-order rate-constant, k_1^{GST}. This could be achieved by feeding with permeant precursors, such as *N*-acetyl cysteine, or by analysing transgenic plants expressing cytoplasmic γ-glutamylcysteine synthetase which show elevated cytoplasmic GSH levels (Noctor *et al.*, 1996). The situation for the GSX-pump is slightly more straightforward, as measurement below its apparent K_m would only require lower levels of cytoplasmic GSB that can be readily achieved by lowering the concentration of MCB used to drive the conjugation reaction. Equally, however, the substantial amount of effort required to conduct such analyses has to be carefully weighed against the additional value of the information gained within the context of the original biological question.

On the more positive side, simulation modelling offers a powerful and flexible tool to link information from different sources and produce predictive models that can be subjected to repeated testing and refinement. For example, in the case of the GSH-dependent detoxification pathway, the models developed for MCB could be broadened to encompass other xenobiotics, including herbicides, by incorporating the relative transport activity of the GSX-pump, measured *in vitro* for each substrate by conventional biochemical techniques (Martinoia *et al.*, 1993; Li *et al.*, 1995; Lu *et al.*, 1998). The natural extrapolation of this approach would be to use the information from different experimental systems to develop physiological models, which could be mapped onto a common anatomical framework in the form of a virtual root.

Acknowledgements

We would like to thank Nick Kruger and Peter Darrah for advice during this work and comments on the manuscript, and Nick White for help with the two-photon microscopy. This work was supported by INTAS and Aventis Crop Science.

References

Adams SR, Backsai BJ, Taylor SS, Tsien RY. 1999. Optical probes for cyclic AMP. In: Mason WT, ed. *Fluorescent and luminescent probes for biological activity*, 2nd edn. San Diego: Academic Press, 156–172.

Adams SR, Harootunian AT, Buechler YJ, Taylor SS, Tsien RY. 1991. Fluorescence ratio imaging of cyclic AMP in single cells. *Nature* 349, 694–697.

Baker NR, Oxborough K, Lawson T, Morison JIL. 2001. High resolution imaging of photosynthetic activities of tissues, cells and chloroplasts in leaves. *Journal of Experimental Botany* **52,** 615–621.

Bennett BD, Jetton TL, Ying GT, Magnuson MA, Piston DW. 1996. Quantitative subcellular imaging of glucose metabolism within intact pancreatic islets. *Journal of Biological Chemistry* **271,** 3647–3651.

Blancaflor EB, Gilroy S. 2000. Plant cell biology in the new millenium: new tools and new insights. *American Journal of Botany* **87,** 1547–1560.

Bright GR, Fisher GW, Rogowska J, Taylor DL. 1989. Fluorescence ratio imaging microscopy. *Methods of Cell Biology* **30,** 157–192.

Coleman JOD, Blake-Kalff MMA, Davies TGE. 1997*a*. Detoxification of xenobiotics by plants: chemical modification and vacuolar compartmentation. *Trends in Plant Science* **2,** 144–151.

Coleman JOD, Randall R, Blake-Kalff MMA. 1997*b*. Detoxification of xenobiotics in plant cells by glutathione conjugation and vacuolar compartmentation: a fluorescent assay using monochlorobimane. *Plant, Cell and Environment* **20,** 449–460.

Denk W, Strickler J, Webb WW. 1990. Two-photon laser scanning microscopy. *Science* **248,** 73–76.

Dolan L, Janmaat K, Willemsen V, Linstead P, Poethig S, Roberts K, Scheres B. 1993. Cellular organization of the *Arabidopsis thaliana* root. *Development* **119,** 71–84.

Dolan L, Duckett CM, Grierson C, Linstead P, Schneider K, Lawson E, Dean C, Roberts K. 1994. Clonal relationships and cell patterning in the root epidermis of *Arabidopsis*. *Development* **120,** 2465–2474.

Fricker MD, Errington RJ, Wood J, Tlalka M, May M, White NS. 1997. Quantitative confocal fluorescence measurements in living tissue. In: Van Duijn-and B, Wiltink A, eds. *Signal transduction—single cell techniques*. Berlin: Springer, 413–445.

Fricker MD, May M, Meyer AJ, Sheard NS, White NS. 2000. Measurement of glutathione levels in intact roots of *Arabidopsis*. *Journal of Microscopy* **198,** 162–173.

Genty B, Meyer S. 1994. Quantitative mapping of leaf photosynthesis using chlorophyll fluorescence imaging. *Australian Journal of Plant Physiology* **22,** 277–284.

Gilroy S. 1997. Fluorescence microscopy of living plant cells. *Annual Review of Plant Physiology and Molecular Biology* **48,** 165–190.

Goddard H, Manison NFH, Tomos D, Brownlee C. 2000. Elemental propagation of calcium signals in response-specific patterns determined by environmental stimulus strength. *Proceedings of the National Academy of Sciences, USA* **97,** 1932–1937.

Gray JD, Kolesik P, Hoj PB, Coombe BG. 1999. Confocal measurement of the three-dimensional size and shape of plant paranchyma cells in a developing fruit tissue. *The Plant Journal* **19,** 229–236.

Grynkiewicz G, Poenie M, Tsien RY. 1985. A new generation of calcium indicators with greatly improved fluorescent properties. *Journal of Biological Chemistry* **260,** 3440–3450.

Hanson MR, Köhler RH. 2001. GFP imaging: methodology and application to investigate cellular compartmentation of metabolism in plants. *Journal of Experimental Botany* **52,** 529–539.

Haugland RP. 1999. *Handbook of fluorescent probes and research chemicals*, 7th edn. Molecular probes. Oregon: Eugene.

Heim R, Tsien RY. 1996. Engineering green fluorescent protein for improved brightness, longer wavelengths and fluorescence resonance energy transfer. *Current Biology* **6,** 178–182.

Hepler PK, Gunning BES. 1998. Confocal fluorescence microscopy of plant cells. *Protoplasma* **201,** 121–157.

Howard CV, Reed MG. 1998. *Unbiased stereology. Three-dimensional measurements in microscopy*. Oxford: Bios Scientific Publishers.

Hutzler P, Fischbach R, Heller W, Jungblut TP, Reuber S, Schmitz R, Veit M, Weissenböck G, Schnitzler J-P. 1998. Tissue localization of phenolic compounds in plants by confocal laser scanning microscopy. *Journal of Experimental Botany* **49,** 953–965.

Jauh G-Y, Phillips TE, Rogers JC. 1999. Tonoplast intrinsic protein isoforms as markers for vacuolar functions. *The Plant Cell* **11,** 1867–1882.

Köckenberger W. 2001. Nuclear magnetic resonance microimaging in the investigation of plant cell metabolism. *Journal of Experimental Botany* **51,** 641–652.

Li Z-S, Zhao Y, Rea PA. 1995. Magnesium adenosine 5′-triphosphate energizes transport of glutathione-*S*-conjugates by plant vacuolar membrane vesicles. *Plant Physiology* **107,** 1257–1268.

Lu YP, Li Z-S, Drodowicz YM, Hortensteiner S, Martinoia E, Rea PA. 1998. AtMRP2, an *Arabidopsis* ATP binding cassette transporter able to transport glutathione S-conjugates and chlorophyll catabolites: functional comparisons with AtMRP1. *The Plant Cell* **10,** 267–282.

Martinoia E, Grill E, Tommasini R, Kreuz K, Amrhein N. 1993. ATP-dependent glutathione *S*-conjugate 'export' pump in the vacuolar membrane of plants. *Nature* **364,** 247–249.

May MJ, Vernoux T, Leaver CJ, Van Montagu M, Inzé D. 1998. Glutathione homeostasis in plants: implications for environmental sensing and plant development. *Journal of Experimental Botany* **49,** 649–667.

Meyer AJ, Fricker MD. 2000. Direct measurement of glutathione in epidermal cells of intact *Arabidopsis* roots by two-photon laser scanning microscopy. *Journal of Microscopy* **198,** 174–181.

Miyawaki A, Llopis J, Heim R, McCaffery JM, Adams JA, Ikura M, Tsien RY. 1997. Fluorescent indicators for calcium based on green fluorescent protein and calmodulin. *Nature* **388,** 882–887.

Miyawaki A, Griesback O, Heim R, Tsien RY. 1999. Dynamic and quantitative Ca^{2+} measurements using improved cameleons. *Proceedings of the National Academy of Sciences, USA* **96,** 2135–1240.

Noctor G, Strohm M, Jouanin L, Kunert KK, Foyer CH, Rennenberg H. 1996. Synthesis of glutathione in leaves of transgenic poplar over expressing γ-glutamylcysteine synthetase. *Plant Physiology* **112,** 1071–1078.

Oxborough K, Baker NR. 1997. An instrument capable of imaging chlorophyll *a* fluorescence from intact leaves at very low irradiance and at cellular and subcellular levels of organization. *Plant, Cell and Environment* **20,** 1473–2483.

Pawley JB. 1995. *Handbook of biological confocal microscopy*, 2nd edn. New York: Plenum Press.

Paris N, Stanley CM, Jones RL, Rogers JC. 1996. Plant cells contain two functionally distinct vacuolar compartments. *Cell* **85,** 563–572.

Piston DW. 1999. Imaging living cells and tissues by two-photon excitation microscopy. *TICB* **9,** 66–69.

Piston DW, Masters BR, Webb WW. 1995. Three-dimensionally resolved NAD(P)H cellular metabolic redox imaging of the *in situ* cornea with two-photon excitation laser scanning microscopy. *Journal of Microscopy* **178,** 20–27.

Rea PA, Li Z-S, Lu YP, Drozdowicz YM, Martinoia E. 1998. From vacuolar GS-X pumps to multispecific ABC transporters. *Annual Review of Plant Physiology and Molecular Biology* **49,** 727–760.

Roberts JKM, Callis J, Wemmer D, Walbot V, Jardetzky O. 1984. Mechanism of cytoplasmic pH regulation in hypoxic maize root tips and its role in survival under hypoxia. *Proceedings of the National Academy of Sciences, USA* **81,** 3379–3383.

Roos W. 2000. Ion mapping in plant cells—methods and applications in signal transduction research. *Planta* **210,** 247–370.

Swanson SJ, Bethke P, Jones RL. 1998. Barley aleurone cells contain two types of vacuoles: characterization of lytic organelles by use of fluorescent probes. *The Plant Cell* **10,** 685–698.

Tlalka M, Runquist M, Fricker MD. 1999. Light perception and the role of the xanthophyll cycle in blue-light-dependent chloroplast movements in *Lemna trisulca* L. *The Plant Journal* **20,** 447–459.

Török P, Hewlett SJ, Varga P. 1997. The role of specimen-induced spherical aberration in confocal microscopy. *Journal of Microscopy* **188,** 158–172.

White NS, Errington RJ, Fricker MD, Wood JL. 1996. Aberration control in quantitative imaging of botanical specimens by multidimensional fluorescence microscopy. *Journal of Microscopy* **181,** 99–116.